IOP Publishing Phys. Biol. 14 (2017) 015003 doi:10.1088/1478-3975/aa5698

Physical Biology

OPEN ACCESS

PAPER

On the micro-indentation of plant cells in a tissue context

Gabriella Mosca[1,2], Aleksandra Sapala[1], Soeren Strauss[1], Anne-Lise Routier-Kierzkowska[1] and Richard S Smith[1,2]

[1] Department of Comparative Development and Genetics, Max Planck Institute for Plant Breeding Research, Cologne, Germany
[2] Institute of Plant Sciences, University of Bern, Bern, Switzerland

E-mail: smith@mpipz.mpg.de

RECEIVED
16 August 2016

REVISED
28 November 2016

ACCEPTED FOR PUBLICATION
4 January 2017

PUBLISHED
8 February 2017

Keywords: plant biomechanics, finite element method, micro-indentation, cellular force microscopy, morphogenesis, 3D cellular tissue

Supplementary material for this article is available online

Abstract

The effect of geometry on cell stiffness measured with micro-indentation techniques has been explored in single cells, however it is unclear if results on single cells can be readily transferred to indentation experiments performed on a tissue *in vivo*. Here we explored this question by using simulation models of osmotic treatments and micro-indentation experiments on 3D multicellular tissues with the finite element method. We found that the cellular context does affect measured cell stiffness, and that several cells of context in each direction are required for optimal results. We applied the model to micro-indentation data obtained with cellular force microscopy on the sepal of *A. thaliana*, and found that differences in measured stiffness could be explained by cellular geometry, and do not necessarily indicate differences in cell wall material properties or turgor pressure.

1. Introduction

Growth in plant cells is a physical process that results from a complex interplay of gene regulation and mechanics. Plant cell growth is thought to be primarily driven by a relaxation process that releases stress in the cell wall (Cosgrove (1993a), Cosgrove 2005, Geitmann and Ortega 2009). Turgor pressure within the cell stretches the wall elastically, and this elastic strain is made plastic by cell wall remodeling enzymes under the control of genetic regulatory networks. The interplay between stress and growth factors can been seen in the Lockhart model (Lockhart 1965), where the growth rate is presented as a function of both turgor pressure, which induces stress and strain in the cell wall, and stress relaxation or extensibility, which is controlled by molecular networks.

The regulation of growth thus depends both on the stress in the wall, as well as growth promoting biochemical factors. This suggests that cells under more stress (and strain) should grow faster in similar biochemical conditions, an idea that has experimental support (Cosgrove (1993b), Zerzour *et al* 2009). The direct relationship between stress and plant cell growth implies that morphogenesis not only depends on cell wall remodeling enzymes, but also on factors that can change stress in the cell wall, such as tugor pressure and cell geometry. In single cells with simple shapes it is possible to calculate stresses directly (Weber *et al* 2015), if the geometry and the pressure are known. However in a tissue, the effect of neighbor cells also plays a role (Bassel *et al* 2014). Understanding the impact of stresses in a tissue context is thus essential for the understanding of how growth is regulated during morphogenesis of multicellular tissues.

In addition to the passive feedback of stress on growth inherent in the stress relaxation model, there is also evidence for more active feedbacks. Cortical microtubules have been proposed to act as a stress sensor in plants (Hejnowicz *et al* 2000, Hamant *et al* 2008, Jacques *et al* 2013, Sampathkumar *et al* 2014), with their reorientation sensitive to the direction of maximal stress. Since the cortical microtubules direct the cellulose synthase (Paredez *et al* 2006), they can influence both the strength and anisotropy of the cell wall affecting cell shape. Cell shape in turn affects the stress, providing a mechanism for a stress-dependent feedback loop.

It is possible to directly measure turgor pressure in a cell with a pressure probe (Tomos and Leigh 1999). The method involves puncturing the cell wall with a microcapillar needle filled with oil attached to a pressure transducer that is able to directly measure the

pressure of the vacuole. The main disadvantages of this technique are that it can only be used on large cells, and that it is invasive and usually kills the cell after the measurement. A less invasive method for the estimation of turgor pressure is ball tonometry (Lintilhac *et al* 2000). In this method an indentation is performed with a large, spherical probe with a diameter comparable to the cell size. Both the reaction force and the contact patch are recorded during indentation. Under the hypothesis that pressure is the dominating factor in this kind of indentation, the reaction force will be proportional to the turgor pressure and the projected contact area. Wang *et al* (2006) reproduced this result for indentation on suspension cultured tomato cells, and compared their indentation results with pressure probe measurements and found good agreement. The method depends on the ability to accurately measure the contact area during indentation, which can be difficult in practice.

Atomic force microscopy (AFM) indentation experiments have also been used in plants to measure cell wall stiffness and/or turgor pressure (Milani *et al* 2011, Peaucelle *et al* 2011, 2015, Sampathkumar *et al* 2014). A cantilever probe is lowered onto the sample, and the deflection of the cantilever used to calculate a force-indentation curve. AFM usually operates in the nanoscale, both for indenter size, indentation depth and force (Milani *et al* 2011, Sampathkumar *et al* 2014). Some authors have extended this range by using very stiff cantilevers with large tips or by gluing beads to the tip (Peaucelle *et al* 2011). A commonly used model to interpret AFM indentation experiments is the Hertz model (Johnson and Johnson 1987, Hertz 1993, Chen 2014), that gives an analytical solution for the force-indentation curve for the contact of two spheres of homogeneous, isotropic material. The substrate is given a very large radius, making it effectively flat. This assumption, combined with other modifications, can be used to adapt the model for indentation with both pyramidal and conical indenter shapes. The indentation depth must be much smaller than the thickness of the sample and there must be homogeneous, isotropic, linear elastic material properties with negligible prestress.

Another technique is based on a dynamic mechanical analysis at nanoscale (nanoDMA) (Hayot *et al* 2012, Forouzesh *et al* 2013) where a small oscillatory force with a given frequency is applied with a tip to the sample and the deformation is plotted over time. Combined with a finite element method (FEM) model of the sample, the viscoelastic properties can be inferred.

An analytic method for simple cell geometry has been developed that allows the extraction of both pressure and Young's modulus from AFM indentation (Beauzamy *et al* 2015), by extending previous work by Vella *et al* (2012) from spherical to ellipsoid shaped cells. The slope of the force-indentation curve for a very small indentation depth (compared to the wall thickness) is measured, and by application of the Hertz contact model, the cell wall Young's modulus is calculated. Then the slope at a deeper indentation depth, comparable to the wall thickness, is computed. The surface surrounding the indentation point is approximated by an ellipsoid over a height corresponding to the indentation depth, and a mathematical relation connecting the Young's modulus, curvature and linear stiffness provides the turgor pressure. One key assumption with this approach is that the cell wall is isotropic and that its in-plane stiffness is comparable to that in the direction normal to the surface.

Cellular force microscopy (CFM) (Routier-Kierzkowska *et al* 2012, Vogler *et al* 2013, Routier-Kierzkowska and Smith 2014) is an indentation technique like AFM, but typically acts at a scale several orders of magnitude larger for indentation depth and indenter radius (normally micrometer scale), and forces (normally 10s of micro-Newtons). When combined with plasmolysis experiments (osmotic treatments) to measure cell deformation upon release of turgor pressure, it has been used to estimate both cell wall material properties and turgor pressure without killing the cell (Weber *et al* 2015). It was found that in single turgid plant cells, the indentation force was most sensitive to the cell geometry and pressure, rather than the cell wall material properties. However the stretch ratios observed during osmotic treatments are highly sensitive to elastic properties, and when combined with indentation results they can be used to fit an FEM model of cell pressurization and indentation to obtain estimates for both turgor pressure and cell wall elasticity, including anisotropy (Weber *et al* 2015, Hofhuis *et al* 2016). A review of the techniques to assess cell wall material properties and turgor pressure can be found in Milani *et al* (2013).

In this paper we extend the work of Weber *et al* (2015) from single cells to a three dimensional tissue of interconnected cells. Since plant cell walls are rigidly bound to their neighbors, a pressurized plant tissue results in stresses that are non trivial. To understand this complexity we performed FEM simulations of cell indentation and osmotic treatments on templates representing 3D tissues of interconnected cells, and explored how different material properties, geometry, and the arrangements of cells affect the indentation stiffness measured with the CFM probe.

2. Methods

In our simplified tissue, we started with a reference layout of staggered boxes of identical cells of size $20 \times 20 \times 20$ μm with smoothed corners (figure 1). The sizes have been chosen to be intermediate between small meristematic cells, about 5 μm in diameter, and larger more differentiated cells, such as hypocotyl cells that can be several hundreds of microns in length in *Arabidopsis thaliana* (Gendreau *et al* 1997). The templates are named as follows. S-X-Y-Z denotes a staggered template with X cells in the x direction, Y in y,

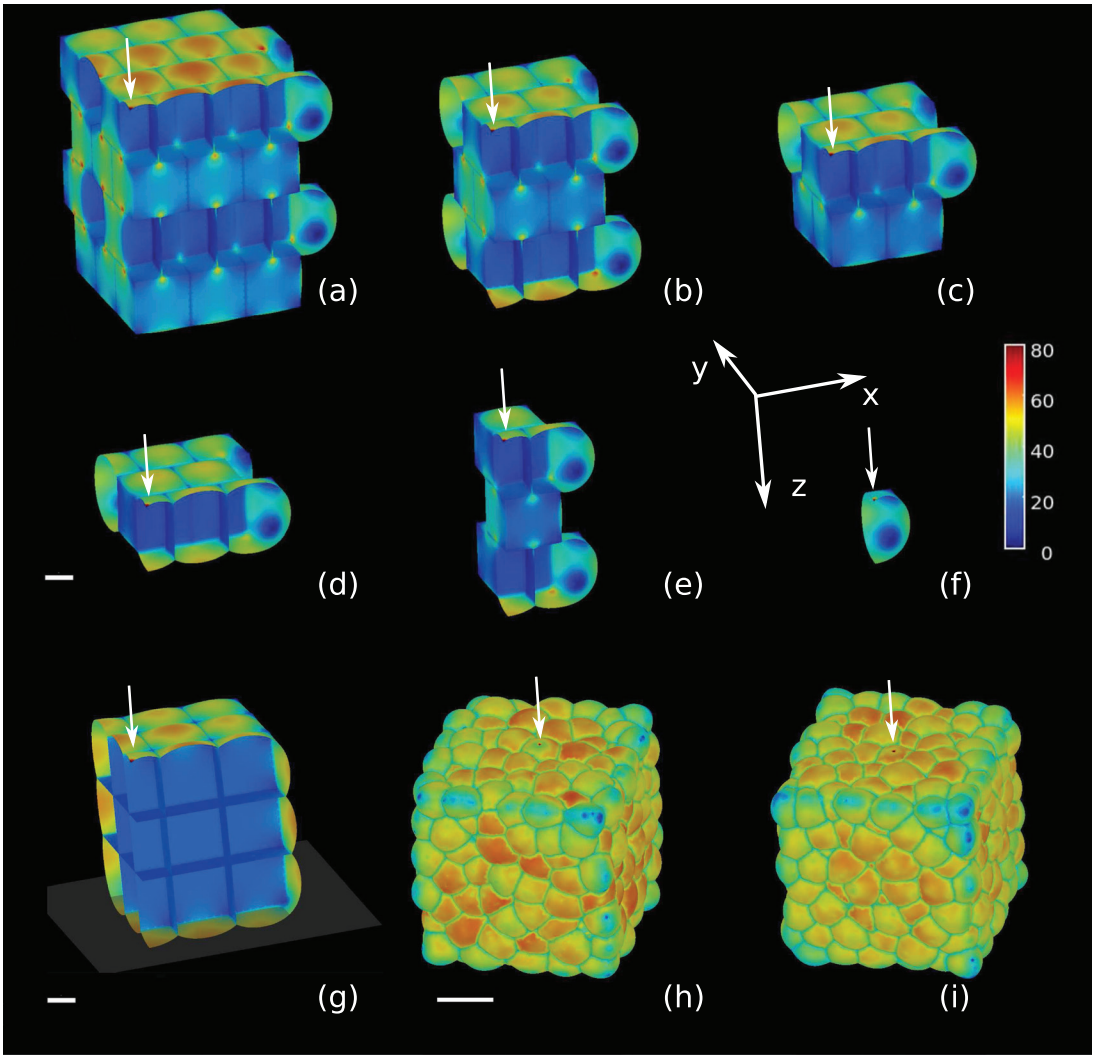

Figure 1. Different templates used for indentation simulations. Only a quarter of the template needs to be simulated due to symmetry and the white arrows indicate the location of the indenter. (a) S-7-7-4 template, (b) S-5-5-3 template, (c) S-5-5-2 template, (d) S-5-5-1 template (e) S-3-3-3 template, (f) S-1-1-1 free template, (g) N-5-5-3 template. The white arrow represents the indenter and the grey plane represents the part of template fixed during indentation as if submerged in a stiff agarose layer. Each square cell has a side of 20 μm. (h) Random template made with Voronoi cells 1, (i) random template made with Voronoi cells 2. The heat-map shows the trace of Cauchy stresses with a linear color map restricted to the range 0–80 MPa. Scalebar for (a)–(g) 20 μm, for (h)–(i) 50 μm.

and Z in the z direction. N-X-Y-Z denotes a non staggered template. The cell wall thickness t used was 0.25 μm, which is within the range of those reported for the *Arabidopsis* hypocotyl of 50 nm to 1 μm (Derbyshire *et al* 2007). FEM simulations were performed with our own custom FEM software that has been developed to model pressurized plant cells (Bassel *et al* 2014). This framework supports large strains and large deformations/rotations. We modeled the cell walls with an isotropic, homogeneous Saint Venant–Kirchhoff material law that depends only on the Young's modulus E and Poisson's ratio ν. Although the Poisson's ratio has not been measured in *Arabidopsis*, Wei *et al* (2001) have measured it for onion leaf epidermis and found values in the range of 0.18–0.3. Accordingly a value of 0.2 was used by Hamant *et al* (2008). Other authors assume that the Poisson's ratio is close to full incompressibility and set it to 0.5 for isotropic material (Milani *et al* 2011, Peaucelle *et al* 2011). Weber *et al* (2015) have shown that indentation force is not very sensitive to the Poisson's ratio for the indentation of single cells. In our simulations we used a value of $\nu = 0.3$. In supplementary figure 1.1 (stacks.iop.org/PhysBio/14/015003/mmedia) we show the effect on the indentation curves for our chosen Poisson's ratio and the fully compressible case, $\nu = 0$. The results show that the difference is negligible. It is though important to bear in mind that two materials identical but for the Poisson ratios will not be stretched in the same way under the action of turgor pressure. For pressure P and Young's modulus E, we chose values in line with previous measurements (Chanliaud *et al* 2002, Wang *et al* 2006, Forouzesh *et al* 2013), setting $P = 0.5$ MPa and $E = 200$ MPa. The simulations were performed with our in-house FEM code (Bassel *et al* 2014) that uses an explicit method that is stable with respect to buckling that can occur when inflating complex structures to high pressure, or when indenting

thin shells (Nasto *et al* 2013). In the case of buckling, the method is able to reach an energy minimum, which may not be the global minimum, but still represents a typical configuration that would be obtained in reality. The simulation loop finds the equilibrium state by using a pseudo time-stepping technique. At each iteration the residual nodal forces due to internal stresses and boundary loads will move the points down the gradient of the total potential energy of the system. For well behaved systems the method is significantly slower than direct methods, so we use a GPU-based solver to achieve reasonable computation times (Bassel *et al* 2014). All models in this analysis except the two random templates (see figures 1(h) and (i)) present two symmetry planes, the *xz*-plane and the *yz*-plane, so that only a quarter of the model template is required for the simulation. Centering the template in the axis origin, we imposed symmetry conditions along these planes. A symmetry condition is realized by fixing individual degrees of freedom. For the *xz*-plane, we fix displacements in *y* for the selected nodes, and for *yz*-plane we fix displacements in *x*. The initial template is constructed with an array of boxes with straight edges. Since plasmolised cells do not have sharp corners, we slightly pre-inflate the cells with a pressure of $P = 0.01$ MPa and a Young's modulus of 5000 MPa. The mesh resulting from this simulation is then used as the stress free starting template. The area around the indentation point is refined in order to better approximate the deformation and the reaction force in this location. During indentation experiments, samples are typically supported by a layer of stiff agarose. To approximate this condition we assumed that the points on the bottom surface (i.e. below a certain height, 1.8 μm for the reference simulation) are in contact with the agarose and are labeled as bottom points (figure 1(g)). The template is then inflated to the prescribed pressure. Upon reaching equilibrium the points that were assigned as bottom points are now fixed in all their degrees of freedom.

We modeled two types of indenter contact, a rigid spherical tip and a point force. Point indentation assumes that all the force is exerted on a single node, whereas for a spherical indenter this force is spread over the nodes within the radius of the indenter. Indentations were performed at the center of the periclinal wall of the central cell of the template. The indentation point for all the templates was the surface point at the intersection of the *xz* and *yz* symmetry planes (see figure 1(g)). The degree of freedom in *z* direction of the indentation point was fixed and set to the indentation required. At each time step, points in the vicinity of the indenter were tested for indenter penetration, and moved to the surface of the indenter. This was done by fixing their position in *z*. The *x* and *y* degrees of freedom were left free. If a negative *z*-force acting on any of these points arose during the indentation, then the *z* degree of freedom was released. As the indenter was moved, the reaction force in *z* on the indented nodes was recorded and multiplied by a factor 4 to account for symmetry, giving the reaction force for the indentation.

Table 1. Various stiffness analyses all evaluated around 2 μm depth of the indentation curve.

Analytical solution comparison for sphere, radius 10 μm		
Simulation tool	Stiffness (N m^{-1})	Rel stiff diff (%)
Our FEM simulation	8.36	Reference
Vella's analytic solution	8.78	−4.8
Abaqus comparison on a box, 20 μm side		
Simulation tool	Stiffness (N m^{-1})	Rel stiff diff (%)
Our FEM simulation	13.79	Reference
Abaqus FEM simulation	13.31	−3.47
Mesh refinement analysis, template S-5-5-3 box side 20 μm		
Number of nodes	Stiffness (N m^{-1})	Rel stiff diff (%)
48 220	15.32	Reference
192 256	15.25	0.4
Indenter size analysis, template S-5-5-3 box side 20 μm		
Indenter radius μm	Stiffness (N m^{-1})	Rel stiff diff (%)
1	15.32	Reference
Point indentation	13.98	−8.7
0.5	14.61	−4.6
2	16.46	7.4

3. Validation

Previous work suggests that for typical cell wall thicknesses, bending stiffness is negligible for turgid plant cells (Bozorg *et al* 2014, Weber *et al* 2015). This justifies our development of a finite element code using triangular membrane elements (Bassel *et al* 2014). We tested both its correctness, and whether the membrane hypothesis was acceptable under our simulation conditions. First we compared our code against a method that gives an implicit analytical expression for the reaction force for point indentation on thin spherical shells (Vella *et al* 2011) (also a membrane formulation). The implicit formula given in equations (4.1) and (4.2) in Vella *et al* (2011) was integrated numerically for the case $\nu = 0.0$, giving an explicit relation between force and indentation. The comparison to our simulation is reported in table 1. In the FEM simulation a point indentation can be represented as a concentrated nodal load or force, however this is not physical and will have an intrinsic dependence on the mesh size. Although the effect is relatively mild on pressurized shells, the dependence on mesh triangle size can be seen in next section on mesh resolution convergence analysis. Even when the mesh is very fine, further mesh refinements still cause the reaction force and stiffness to drop slightly. In order to circumvent this problem, while trying to match the analytical simulation, we opted for a finite contact area with a small indenter radius of 0.15 μm. The comparison to our simulation

Table 2. Sensitivity analysis for different cell templates in a staggered arrangement. The cells are 20 μm boxes with stiffness evaluated at approximately 2 μm indentation depth.

Template analysis—Staggered case						
Template	Stiffness (N m^{-1})	Rel stiff diff (%)	Volume ratio	Rel vol diff (%)	Linear long strain (%)	Relative strain diff (%)
S-7-7-5	15.79	Reference	1.29	Reference	5.5	Reference
S-7-7-4	16.00	1.36	1.29	0	5.0	−8.8
S-5-5-3	15.33	−2.93	1.26	−10.3	5.6	2.2
S-5-5-2	15.71	−0.39	1.26	−10.3	4.6	−16.1
S-5-5-1	15.01	−4.96	1.26	−10.3	3.0	−45.3
S-3-3-3	14.34	−9.2	1.23	−20.7	5.0	−8.8
S-1-1-1 free	12.03	−24.83	1.5	72.4	13.0	137
S-1-1-1 blocked	13.36	−16.54	1.22	−24.1	—	—

is reported in table 1 and the two indentation curves are also included in supplementary figure 1.1. For the sphere the curves are not yet linear around 2 μm indentation depth so we have computed their stiffness along a smaller interval (2.5–2 μm indentation depth). We also computed the stretch ratios analytically for the case of full compressibility ($\nu = 0$) and found our simulation for the sphere in agreement within 0.1% with the analytical prediction (see supplementary section 1.2 for the analytical derivation).

Next we tested our simulations against the commercial FEM software, Abaqus (www.3ds.com/products-services/simulia/products/abaqus/). We used a finite radius (1 μm) contact indentation on a box which represents features close to our cell shape. Although our simulations used linear elements, we had fewer problems with convergence in Abaqus standard using quadratic quadrilateral shell elements (8-node doubly curved thick shell, reduced integration, S8R). The mesh resolution for Abaqus and our code were comparable. Material parameters and thickness were the same for all simulations for our test cases. We computed the linear stiffness of indentation at 2 μm indentation depth as the reaction force at 2.5 μm indentation depth minus the reaction force at 1.5 μm. Note that the force-indentation curve is linear in this range (see supplementary figure 1.2). The results are summarized in table 1. Considering the experimental variability *in vivo*, we assume that variations smaller than 5% are negligible, and thus we conclude that our simulation code is valid within the range of interest and that the membrane hypothesis is accurate enough. When simulating low pressure samples where bending stiffness becomes more significant, a shell formulation would likely be required.

In order to check if the mesh refinement was accurate enough for our simulations we started with the reference template S-5-5-3 with a cell size of $20 \times 20 \times 20$ μm (see figure 1(b)). We chose a spherical indenter of 1 μm radius. Table 1 shows the results of the mesh refinement test. The mesh with 48 220 nodes had triangles with a length of about 0.6 μm near the indentation area, while the mesh with 192 256 nodes had a length of 0.3 μm. We thus concluded that the mesh with the element length of 0.6 μm, when coupled with a spherical indenter of 1 μm in radius, is fine enough for our analysis. Other templates will use the same degree of accuracy.

4. Results and discussion

In AFM experiments with nanometer scale indentations smaller than cell wall thickness, the interpretation is often done with hertz-type models, which take into account indenter size and shape when fitting the force-indentation curves (Milani *et al* 2011, Beauzamy *et al* 2015). CFM indentation involves larger tips in the 1–2 μm range with indentation depths of several microns (Routier-Kierzkowska and Smith 2013) or more. Previously Weber *et al* (2015) showed that CFM indentation is not very sensitive to indenter radius in this regime when measuring the indentation stiffness of turgid cells. Here we repeated this analysis for our tissue by performing simulations with various indenter sizes, including point indentation, on the same template used for the mesh sensitivity analysis. From table 1 we see that the effect of indenter size is mild, but not negligible. The results show that one should try to measure the indenter size with some accuracy, although for a 100% indenter radius change, the stiffness varies by only 7%. It is important to bear in mind that mesh refinement around the indenter should be performed in order to reproduce the contact problem with proper accuracy.

In section 2 it was mentioned that point loads are not physical, and that it is difficult to reproduce mathematical point loads in an FEM simulation. Nevertheless, they are simple to implement, can converge quickly, and are useful for comparison with analytical methods. With this in mind we investigated how mesh size affects the accuracy of a point load, and in particular how it relates to a simulation using full indenter contact. We found that the condition that provides the closest results to the full contact model is when the mesh refinement around the indented point is roughly comparable to the indenter radius. This is because the force is distributed on a surface comparable to that of the actual indenter. However it should be noted that under this condition, the results show a discrepancy higher than 5% (see table 1).

4.1. Tissue context

In order to analyze the effect of neighbor cells on indentation experiments, we created different templates with a varying number of cells surrounding the indentation. Again we considered a relative stiffness difference of 5% to be the lower limit to treat a variation in stiffness as significant. We started with a template of 7 cells in the *x*-direction by 7 cells in the *y*-direction, by 3 cells in the *z*-direction, so that the indented cell is in a staggered grid surrounded by two cells on each side. We then progressively reduced the layers of cells in the two in-plane directions and the in the depth direction until we were left with a single cell (see figure 1(f)). We compared the results of both the indentation and the volume and stretch ratios from plasmolised (0 pressure) to pressurized cells. The reaction force and stiffness for the different templates is shown in table 2. For the single cell there are 2 different boundary conditions. The one marked free has the same boundary conditions as the others, with the bottom fixed and all other sides free to expand. In the single cell blocked simulation, the lateral walls are completely prevented from expanding in the *x*-*y* directions, which we reasoned might provide a simple method to simulate the presence of neighbouring cells. Templates S-5-5-3, S-5-5-2, S-5-5-1 differ in stiffness from the reference template by less than 5%, below our threshold for significance. Surprisingly, template S-5-5-2 has closer stiffness to the initial reference template than S-5-5-3. Note that S-5-5-3 and S-5-5-1 are also close in stiffness, suggesting that the ratio of packed versus half free cells under the indenter due to the staggered arrangement may be the cause. The template alternates between open cavity and cell wall directly under the indenter, as can be seen in figure 1. When the ratio of cell wall to open cavity under the indenter is higher, the indentation stiffness will be higher. This oscillatory effect gets smaller as the template gets deeper.

To test this hypothesis we created a series of non-staggered templates and performed the same analysis as in table 2, with the results reported in table 3. For the non-staggered arrangement the oscillatory behavior of the stiffness for odd-even in-depth layers of cells is not present, and beyond 2 layers, adding cells does not make a difference. Figures 1(b) and (g) show the staggered versus the non-staggered arrangement of cells for the 5-5-3 template. The difference gets dramatic in the case of a single cell for both the free and blocked case. This shows that preventing the lateral walls from expanding in the *xy*-direction is not a good enough approximation for the presence of surrounding cells.

Linear 1D strain variation (table 2) shows that modeling one single layer of cells in depth (S-5-5-1) has a significant impact on the longitudinal strain, so that it is advisable to model at least two layers of cells in depth when possible. Strain and/or volume ratio variations in table 2 are high as well for S-3-3-3 and the single cell cases, where stiffness variations are high already. We conclude that isolated cells are not a good proxy for tissue indentation experiments, whether the side walls are blocked or not. However, only a few cells of mechanical context are required in each direction to reasonably simulate a full tissue. We therefore chose S-5-5-3 as our reference template for further analysis.

Table 3. Stiffness values and relative stiffness differences for cell templates in a non-staggered arrangement. The cells are 20 μm boxes with stiffness measured at approximately 2 μm indentation depth.

Non Staggered case—stiffness analysis		
Template	Stiffness (N m^{-1})	Rel stiff diff (%)
N-7-7-4	16.16	Reference
N-5-5-4	15.76	−2.4
N-5-5-3	15.76	−2.5
N-5-5-2	15.43	−4.5
N-5-5-1	14.5	−10.3
N-3-3-3	14.84	−8.1

Table 4. Stiffness values and relative stiffness difference for templates with different cell sizes. The arrangement is S-5-5-3 and the reference size for cells is a cube of 20 μm as side. The bottom panel reports stiffness and relative stiffness difference for two 3D Voronoi templates generated with random variation in cell size and neighborhood. In all cases approximately 2 μm indentation depth is used.

Size variation		
Size in *x*-*y*-*z* μm	Stiffness N m^{-1}	Rel stiff diff (%)
One single dimension doubling		
20-20-20	15.33	Reference
20-20-40	17.89	16.68
20-40-20	17.00	10.86
40-20-20	17.91	16.83
Two dimensions doubling		
40-40-20	19.11	24.68
20-40-40	19.33	26.12
40-20-40	20.4	33.07
Three dimensions doubling		
40-40-40	22.31	45.54
Small Size variation		
Size in *x*-*y*-*z* μm	Stiffness N m^{-1}	Rel stiff diff (%)
One single dimension variation (25%)		
25-20-20	15.81	3.15
20-25-20	15.82	3.22
20-20-25	16.06	4.73
Natural variation of linear stiffness for the templates of figures 1(h) and (i)		
Template	Stiffness (N m^{-1})	Rel stiff diff (%)
Random 1	15.13	Reference
Random 2	13.64	−9.85

4.2. Sensitivity to cell size

Starting with S-5-5-3 as the reference template, with cell sizes of $20 \times 20 \times 20$ μm, we doubled the size of each cell in the template in *x*, *y* and *z* and all the combinations up to symmetry. Note that changing the size of a cell will also affect its final curvature and

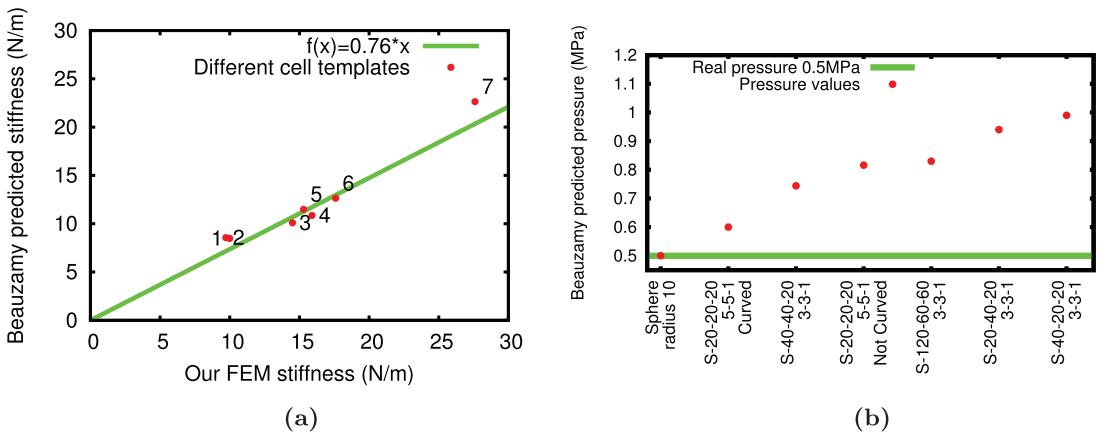

Figure 2. (a) Predicted stiffness using the model of Beauzamy *et al* (2015) at 2 μm indentation depth for material properties $P = 0.5$ MPa, $E = 200$ MPa, $\nu = 0.3$, compared to the FEM simulated stiffness with the same parameters for the different templates. (1) Sphere-radius-10 μm, (2) S-20-20-20-5-5-1-Curved, (3) S-20-20-20-5-5-1-Not Curved, (4) S-40-20-20-3-3-1, (5) S-20-40-20-3-3-1, (6) S-40-40-20-3-3-1, (7) S-120-60-60-3-3-1. (b) Pressure predictions for different templates using the model of Beauzamy *et al* (2015). Green line repsresents the pressure used in the FEM model of 0.5 MPa.

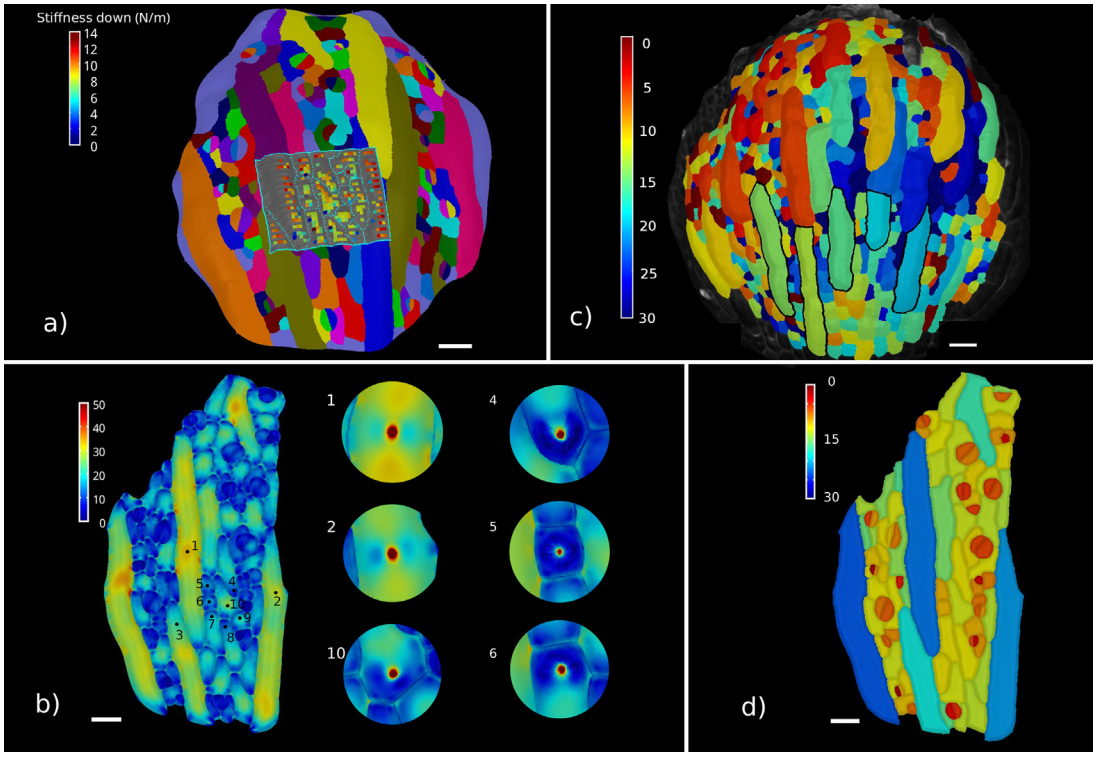

Figure 3. CFM indentation and osmotic treatments on an *A. thaliana* sepal. (a) CFM indentation experimental data superimposed on the 2.5D cell surface mesh generated in MorphoGraphX from confocal microscopy images of the sepal. Heat map color represents the linear stiffness (N m^{-1}). (b) FEM simulation results obtained on a template derived from the image in (a). Material parameters used were $E = 200$ MPa, $P = 0.5$ MPa, and $\nu = .3$. Heat map color indicates the trace of Cauchy stress capped at 50 MPa. The left panel shows the template after inflation and prior to indentation, while the right panel shows a magnification of the area around some of the indentation points. (c) Experimental surface shrinkage data in percentage $(100 \times \frac{\text{InflatedSurface-PlasmolyzedSurface}}{\text{InflatedSurface}})$ from a sepal at a comparable developmental stage as the one in (a). The cells in a position comparable to the indented ones are outlined in black. (d) Volume shrinkage ratio in percentage $100 \times \frac{\text{InflatedVolume-PlasmolyzedVolume}}{\text{InflatedVolume}}$) from the same simulation as in (b). Scalebar 20 μm.

stretch ratios. The results are shown in table 4 where it can be seen that doubling a single dimension increases the stiffness by about 11–17%. Surprisingly, there is a significant difference between the x and y dimensions, that is caused by the arrangement of the cells in files running along the x direction. Note that the stiffness is higher if the cells are made longer along the cell file direction. Cell depth matters as much as length and width, suggesting that drum models, where only the top surface of the cell is modeled, are not an accurate proxy for indentation on a 3D tissue. If two dimensions are doubled together there is an additive

increase in stiffness that ranges between 24–33%. If all three dimensions are doubled, then the stiffness increase is over 45%. Thus cell size plays an important role in the force and stiffness measured by indentation experiments. Interpreting such experiments requires an accurate measure of cell shape including its depth. For very low turgor pressure, cells could become more compliant with increasing size. However, this is never the case for healthy plant cells.

Next we explored indentation sensitivity to smaller size changes, compatible with the uncertainty typically present in real experiments. We performed a size variation of 25% in each direction and report the results in table 4. The data show that even though it is important to be able to quantify the size of cells in all directions, small uncertainties will not have a major effect on the outcome. Again somewhat unintuitive is the sensitivity of the stiffness to the cell size in z.

Next we asked if the exact cell shape and connectivity with respect to the surrounding cells are important factors when fitting indentation data or if simplification of templates based on average values suffice for good estimates. We generated two templates with random variations in average cell size and number of neighbors for the indented cell. The template consisted of Voronoi cells with an average size of 20 μm and arranged in a block with 5–6 cells per side for each template. We indented the center of a central cell on the top of each template after inflation according to the procedure described in section 2. Figures 1(h) and (i) shows their final shape and stress pattern after pressurization and indentation. As we can see from table 4, the specific cell sizes about the indentation significantly affect the results.

4.3. The effect of surface curvature on measured stiffness

Beauzamy *et al* (2015) found that, under certain experimental conditions, curvature alone is the dominant geometric property in the interpretation of AFM indentation experiments. They extracted the Young's modulus of the sample using a Hertz model fitted to the initial part of the indentation curve where the indentation depth was much smaller than cell wall thickness. Next they measured the Gaussian and mean curvature around the indentation point, and measured the stiffness of the AFM force indentation curve at an indentation depth comparable with the wall thickness where the curve becomes linear. They then combined stiffness, curvature, and Young's modulus into an equation they developed in order to estimate the pressure. In addition to the force-indentation curve, their method requires only that an accurate measure of surface curvature is available, which is straightforward with the AFM. The cell surface must also be well approximated by an ellipsoid over a height corresponding to the indentation depth, and the material by isotropic properties.

Table 5. Average values and their standard deviation for surface shrinkage with respect to the data show in figure 1(c). Inferred values for average width and volume shrinkage, (turgid-plasmolised)/turgid, and for average volume increase, (turgid-plasmolised)/plasmolised.

	Average	Standard deviation
Surface shrinkage (%)	16.51	2.96
Width shrinkage (%)	4.9	3.68
Volume shrinkage$_{P->T}$ (%)	21.4	5.64
Volume increase$_{T->P}$ (%)	27.2	7.17

Given these results, we asked whether the boundary conditions imposed by a multicellular context could affect the relationship between force, pressure and curvature. We also wanted to verify if the method proposed by Beauzamy *et al* (2015) was generally applicable in the CFM context, which has a larger indenter radius and larger indentation depths and forces. Seven different cell templates were generated with variation in cell size, arrangement and initial curvature. We then used MorphoGraphX (de Reuille *et al* 2015) to calculate maximal and minimal curvature around the indentation point from which Gaussian and mean curvature can be derived. The curvatures were calculated after full pressurization but before the indentation. We assigned the reference material properties listed in section 2 to the different templates and performed two comparative analyses. In one case we tested whether the linear stiffness around 2 μm indentation depth in the FEM simulation matches with the linear stiffness predicted by equation (1) in Beauzamy *et al* (2015), with the pressure and material properties are given as input. In the second comparison we analysed the pressure predictions. In our simulations the force-indentation curve is linear at 2 μm indentation, so we used the stiffness from this indentation depth. We solved equation (1) numerically for pressure using the script provided in the supporting material of Beauzamy *et al* (2015). The cells were inflated and indented with the procedure described in section 2. In the case of the isolated sphere, we fixed the bottom half prior to indentation. In order to mimic the experimental conditions in Beauzamy *et al* (2015) we assigned our indenter a radius of 0.5 μm. The mesh resolution around the indentation area was 0.3 μm (average triangle side length). The global mesh resolution was about 0.7 μm. Figure 2(a) shows that the relation between the predicted stiffness from Beauzamy *et al* (2015) and the stiffness obtained from FEM simulations are well fitted by a linear function with angular coefficient 0.76 (asymptotic standard error 3.3%). The linear fit also implies that there is a good correlation between curvature of the cell prior to indentation and linear stiffness. The fact that the slope is not equal to 1 shows that the formula does not predict the right stiffness in the context of CFM indentation experiments in tissues. Figure 2(b) shows how the pressure predictions in the case of multicellular context differ from the

Table 6. Experimental and simulated indentation stiffness results fitted between 2.–1.5 μm indentation depth for the points in figure 3(b).

	Stiffness (N m^{-1})									
	Giant cells			Small cells						
	Point 1	Point 2	Point 3	Point 4	Point 5	Point 6	Point 7	Point 8	Point 9	Point 10
Experimental data	13.7	14.0	12.0	8.6	7.2	7.4	7.4	9.3	9.1	10.7
$E = 200$ MPa, $P = 0.5$ MPa	12.6	12.6	11.4	7.4	7.9	6.68	8.46	10.2	8.58	10.6
		Av. stiff giant cells (N m^{-1})			Av. stiff small cells N m^{-1}			Rel. stiff variation %		
Experimental data		13.3			8.1			64		
$E = 200$ MPa, $P = 0.5$ MPa		12.3			8.2			50		

applied pressure in the FEM simulations up to 100%. The only exception is the case of the isolated sphere, where the predicted stiffness is 8.4 N m^{-1} and the stiffness resulting from the CFM simulation is 8.48 N m^{-1}. This again suggests that the multicellular context plays an important role in indentation experiments, affecting the mathematical relation between curvature and stiffness predicted in the case of a single isolated cell. Although curvature alone does not seem sufficient in a multicellular tissue, the strong correlation suggests that it may be possible to adapt the formula for this purpose.

Figure 2(b) shows the pressure predicted according to equation (1) in Beauzamy *et al* (2015). Inputs to the model are the maximal and minimal curvature of the indented cell after inflation and the linear stiffness as obtained from the FEM simulation.

4.4. Application to the sepal of *A. thaliana*

Indentation experiments were performed on a group of epidermal cells located around the middle of the abaxial sepal of *A. thaliana*. A characteristic feature of this organ is that its epidermis contains endoreduplicated, highly elongated cells (giant cells), randomly interspersed among smaller cells (Roeder *et al* 2010). The linear stiffness data are shown in figure 3(a). The stiffness data have been obtained by fitting with a line the linear part of the force-indentation curve. On average this occurred between 1.5 and 2 μm indentation depth after contact. As it can be observed from figure 3(a), the giant cells (marked as 1 and 2 in figure 3(b)) have on average higher stiffness values than the small cells between them. We asked if this variation in stiffness could be explained by the differences in cell size, or if different material properties, pressure or cell thickness were required. To answer this question we simulated the indentation experiments on a realistic template under the hypothesis of uniform material properties and pressure, with constant cell wall thickness. We then checked if we could observe a similar range of linear stiffness variation when indenting on small and giant cells. To create the template we extracted a 2D mesh of the cell outlines from confocal microscope images using MorphoGraphX, and extruded 7 μm in depth creating a layer of 3D cells. The cells were post processed (smoothed) to more realistically capture their original shape (see supplementary figure 1.4). In the resulting mesh, the giant cells had a final depth of approximately 10 μm and the small cells had a depth of approximately 7 μm. The template had an average triangle side length of about 0.8 μm and was refined near the indentation points so that the element side length was approximately 0.3–0.5 μm. It has been shown in table 1 that this refinement gives accurate enough results. We assigned the sepal a Saint Venant–Kirchhoff isotropic material law with Young's modulus $E = 200$ MPa, Poisson's ratio $\nu = 0.3$, turgor pressure of 0.5 MPa and a uniform cell wall thickness of 0.25 μm. To determine whether these parameters are acceptable to model the sepal, we compared the results of plasmolysis experiments as well as the indentation curves. The experimental stretch ratio data are shown in figure 3(c) and are reported in table 5. The volumetric stretch ratio has been inferred and not measured directly (for more details on the procedure see supplementary section 1.4). We then inflated our template and obtained volumetric stretch ratios as shown in figure 3(d) and compared the values for giant cells with those reported in table 5 which are calculated on the basis of the giant cells marked with a black border in figure 3(c). Given that the Poisson's ratio only slightly affects the indentation results and stretch ratio data (Weber *et al* 2015), we are left with two parameters to match for this model, the Young's modulus and Pressure. We found the data to be in reasonable agreement, differing by about 10%.

Next we performed the indentation simulation. The template was pressurized with only a single point fixed, and upon equilibrium but prior to indentation, the bottom surface of the template was fixed as in the previous simulations. A spherical indenter of 0.7 μm radius was used. We computed the linear stiffness by subtracting the reaction force at 2.0 μm and 1.5 μm indentation depth. Figure 3(d) shows the pressurized template prior to indentation, and the stresses around indentation points upon indentation. Note that the stresses can vary significantly along a single cell due to their irregular shape and boundary effects. In order for the fitting to be accurate, the data from simulated indentation points have to be compared with experimental data belonging to points in similar locations within the cells. We considered only points on relatively flat portions of the cell surface (i.e. perpendicular to the indentation direction) where the stiffness data showed good consistency.

Supplementary figure 1.4 reports some of the experimental indentation curves (a) and the corresponding simulated indentation curves (b) labelled accordingly to the points in figure 3(b). On average we observe a good agreement between experiments and simulation for the range of indentation forces. This, combined with the plasmolysis analysis, allows us to conclude that our material parameter choice, as well as pressure are acceptable to proceed with our analysis.

The indentation curves (see supplementary figure 1.5) also display an acceptable agreement between simulation and experiments in terms of absolute force and stiffness, reproducing the trend for giant cells (indentation points 1,2 and 3 in figure 3(b)) which have a significantly higher stiffness than the small cells (indentation points 4, 5 and 6, 7, 8 and 9 in figure 3(b)). The average stiffness variation for these two groups in the simulation, as reported in table 6, is about 50%, while for the experiments it is around 64%. In table 6 the experimental and simulated stiffness values are also reported for each same point individually. Point 10 is an outlier in the small cell population due to its peculiar shape and is left out of the statistics between small and giant cells. On average we can note that the stiffness for giant cells is slightly underestimated by the simulation. One possible explanation is that our extruded template underestimated the difference in depth between the large and small cells. A template made from a 3D segmentation of the cells could remedy this problem, although methods would need to be developed to simplify the resulting mesh for FEM simulation. Our simulations suggest that geometry can explain the stiffness variations observed in the indentation experiments on abaxial sepal of *A. thaliana*, and that a difference in material properties or turgor pressure is not required to explain the results. The results, though, can not rule out that there is a difference in material properties and/or turgor pressure between the small and big cells given that we made simple assumptions such as linear material properties and isotropicity of the cell wall.

5. Conclusions

Our results show that the simulation of indentation experiments in a tissue context gives better results when several layers of cell context in each direction are provided in the model template. For regular cell shapes and arrangements, we found that a template of 5 by 5 cells in plane, and 3 cells in depth is a good compromise between accuracy of results and computational cost. In particular, we found that it is not sufficient to use single cell models, even with fixed side walls, to model indentation experiments on multicellular tissues. Although we expected cell size to affect the indentation stiffness (Vella *et al* 2011, Weber *et al* 2015), we were surprised to find that the depth of cells contributes as much as the width or length. This suggests that the accurate measurement of cell depth is just as important as the other dimensions. We also found that when doing FEM simulations, a finite size indenter is preferred over point indentation, with the mesh refined such that load is not concentrated on very few nodes.

Our work supports the results obtained by Beauzamy *et al* (2015) which relate indentation stiffness and curvature to pressure. This method is very convenient, since both AFM and CFM are scanning probe methods, and can accurately determine the curvature near the indentation point. Although, for a given pressure, the indentation stiffness predicted by the Beauzamy model is nicely correlated to our FEM simulations, there appears to be a scaling factor that is likely related to boundary conditions and the influence of neighbors in the cellular tissue. Note that most of the variations in our analysis, such as changing cell size and arrangement, will also affect the final inflated curvature of the indented cell.

The minimally invasive nature of both confocal imaging and scanning probe techniques such as AFM and CFM means that it is now possible to obtain an accurate measure of cell shape and size along with cell stiffness measurements *in vivo*. Here we have done this with the epidermis of the *A. thaliana* sepal. Combined with osmotic treatments and FEM modeling, we were able to show that measured differences in cell stiffness could be explained by the cellular geometry, rather than differences in turgor pressure or material properties.

Acknowledgments

Support for this work was provided by the Swiss National Science Foundation SystemsX.ch Plant Growth RTD and iPhD project grant 2010/073, the Bundesministerium für Bildung und Forschung grants 031A492 and 031A494, the Human Frontiers Science Program grant RGP0008/2013, and the Max Planck Society.

References

Bassel G W, Stamm P, Mosca G, de Reuille P B, Gibbs D J, Winter R, Janka A, Holdsworth M J and Smith R S 2014 Mechanical constraints imposed by 3d cellular geometry and arrangement modulate growth patterns in the arabidopsis embryo *Proc. Natl Acad. Sci.* **111** 8685–90

Beauzamy L, Derr J and Boudaoud A 2015 Quantifying hydrostatic pressure in plant cells by using indentation with an atomic force microscope *Biophys. J.* **108** 2448–56

Bozorg B, Krupinski P and Jönsson H 2014 Stress and strain provide positional and directional cues in development *PLoS Comput. Biol.* **10** e1003410

Chanliaud E, Burrows K, Jeronimidis G and Gidley M 2002 Mechanical properties of primary plant cell wall analogues *Planta* **215** 989–96

Chen J 2014 Nanobiomechanics of living cells: a review *Interface Focus* **4** 20130055

Cosgrove D J 1993a How do plant cell walls extend? *Plant physiol.* **102** 1

Cosgrove D J 1993b Wall extensibility: its nature, measurement and relationship to plant cell growth. *New Phytologist* **124** 1–23

Cosgrove D J 2005 Growth of the plant cell wall *Nat. Rev. Mol. Cell Biol.* **6** 850–61

Derbyshire P, Findlay K, McCann M C and Roberts K 2007 Cell elongation in arabidopsis hypocotyls involves dynamic changes in cell wall thickness *J. Exp. Bot.* **58** 2079–89

de Reuille P B *et al* 2015 Morphographx: a platform for quantifying morphogenesis in 4d *eLife* **4** e05864
Forouzesh E, Goel A, Mackenzie S A and Turner J A 2013 *In vivo* extraction of arabidopsis cell turgor pressure using nanoindentation in conjunction with finite element modeling *Plant J.* **73** 509–20
Geitmann A and Ortega J K 2009 Mechanics and modeling of plant cell growth *Trends Plant Sci.* **14** 467–78
Gendreau E, Traas J, Desnos T, Grandjean O, Caboche M and Hofte H 1997 Cellular basis of hypocotyl growth in arabidopsis thaliana *Plant Physiol.* **114** 295–305
Hamant O *et al* 2008 Developmental patterning by mechanical signals in arabidopsis *Science* **322** 1650–5
Hayot C M, Forouzesh E, Goel A, Avramova Z and Turner J A 2012 Viscoelastic properties of cell walls of single living plant cells determined by dynamic nanoindentation *J. Exp. Bot.* **63** 2525–40
Hejnowicz Z, Rusin A and Rusin T 2000 Tensile tissue stress affects the orientation of cortical microtubules in the epidermis of sunflower hypocotyl *J. Plant Growth Regul.* **19** 31–44
Hertz H 1993 über die berührung fester elastischer körper journal für die reine und angewandte mathematik, 1882, no92. JS Field, MV Swain: a simple predictive model for spherical indentation *J. Mater. Res.* **8** 297–306
Hofhuis H *et al* 2016 Morphomechanical innovation drives explosive seed dispersal *Cell* **166** 222–33
Jacques E, Verbelen J P and Vissenberg K 2013 Mechanical stress in arabidopsis leaves orients microtubules in a 'continuous' supracellular pattern *BMC Plant Biol.* **13** 163
Johnson K L and Johnson K L 1987 *Contact Mechanics* (Cambridge: Cambridge University Press)
Lintilhac P M, Wei C, Tanguay J J and Outwater J O 2000 Ball tonometry: a rapid, nondestructive method for measuring cell turgor pressure in thin-walled plant cells *J. Plant Growth Regul.* **19** 90–7
Lockhart J A 1965 An analysis of irreversible plant cell elongation *J. Theor. Biol.* **8** 264–75
Milani P, Braybrook S A and Boudaoud A 2013 Shrinking the hammer: micromechanical approaches to morphogenesis *J. Exp. Bot.* **64** 4651–62
Milani P, Gholamirad M, Traas J, Arnéodo A, Boudaoud A, Argoul F and Hamant O 2011 *In vivo* analysis of local wall stiffness at the shoot apical meristem in arabidopsis using atomic force microscopy *Plant J.* **67** 1116–23
Nasto A, Ajdari A, Lazarus A, Vaziri A and Reis P M 2013 Localization of deformation in thin shells under indentation *Soft Matter* **9** 6796–803
Paredez A R, Somerville C R and Ehrhardt D W 2006 Visualization of cellulose synthase demonstrates functional association with microtubules *Science* **312** 1491–5
Peaucelle A, Braybrook S A, Le Guillou L, Bron E, Kuhlemeier C and Höfte H 2011 Pectin-induced changes in cell wall mechanics underlie organ initiation in arabidopsis *Curr. Biol.* **21** 1720–6
Peaucelle A, Wightman R and Höfte H 2015 The control of growth symmetry breaking in the arabidopsis hypocotyl *Curr. Biol.* **25** 1746–52
Roeder A H K, Chickarmane V, Cunha A, Obara B, Manjunath B S and Meyerowitz E M 2010 Variability in the control of cell division underlies sepal epidermal patterning in arabidopsis thaliana *PLoS Biol.* **8** 1–17
Routier-Kierzkowska A L and Smith R S 2013 Measuring the mechanics of morphogenesis *Curr. Opin. Plant Biol.* **16** 25–32
Routier-Kierzkowska A L and Smith R S 2014 Mechanical measurements on living plant cells by micro-indentation with cellular force microscopy *Plant Cell Morphogenesis: Methods and Protocols* (New York: Springer) **1080** 135–46
Routier-Kierzkowska A L, Weber A, Kochova P, Felekis D, Nelson B J, Kuhlemeier C and Smith R S 2012 Cellular force microscopy for *in vivo* measurements of plant tissue mechanics *Plant Physiol.* **158** 1514–22
Sampathkumar A, Krupinski P, Wightman R, Milani P, Berquand A, Boudaoud A, Hamant O, Jönsson H and Meyerowitz E M 2014 Subcellular and supracellular mechanical stress prescribes cytoskeleton behavior in arabidopsis cotyledon pavement cells *Elife* **3** e01967
Tomos A D and Leigh R A 1999 The pressure probe: a versatile tool in plant cell physiology *Annu. Rev. Plant Biol.* **50** 447–72
Vella D, Ajdari A, Vaziri A and Boudaoud A 2011 The indentation of pressurized elastic shells: from polymeric capsules to yeast cells *J. R. Soc. Interface* **9** 448–55
Vella D, Ajdari A, Vaziri A and Boudaoud A 2012 Indentation of ellipsoidal and cylindrical elastic shells *Phys. Rev. Lett.* **109** 144302
Vogler H *et al* 2013 The pollen tube: a soft shell with a hard core *Plant J.* **73** 617–27
Wang L, Hukin D, Pritchard J and Thomas C 2006 Comparison of plant cell turgor pressure measurement by pressure probe and micromanipulation *Biotechnol. Lett.* **28** 1147–50
Weber A, Braybrook S, Huflejt M, Mosca G, Routier-Kierzkowska A L and Smith R S 2015 Measuring the mechanical properties of plant cells by combining micro-indentation with osmotic treatments *J. Exp. Bot.* **66** 3229–41
Wei C, Lintilhac P M and Tanguay J J 2001 An insight into cell elasticity and load-bearing ability. Measurement and theory *Plant Physiol.* **126** 1129–38
Zerzour R, Kroeger J and Geitmann A 2009 Polar growth in pollen tubes is associated with spatially confined dynamic changes in cell mechanical properties *Developmental Biol.* **334** 437–46